

PAPER

Laser-induced transformation of graphitic materials to two-dimensional graphene-like structures at ambient conditions

To cite this article: Aspasia Antonelou *et al* 2018 *Nanotechnology* **29** 384001

View the [article online](#) for updates and enhancements.

You may also like

- [Chaotic behavior of new experimental data of the LTGP \(2004-2006\) confirm possible relation to seismic activity in Western Greece](#)
K Giannakopoulos and A Ifantis
- [Exploiting unsupervised and supervised classification for segmentation of the pathological lung in CT](#)
P Korfiatis, C Kalogeropoulou, D Daoussis *et al.*
- [Integrating multiscale polar active contours and region growing for microcalcifications segmentation in mammography](#)
N S Arikidis, A Karahaliou, S Skiadopoulos *et al.*



ECS The Electrochemical Society
Advancing solid state & electrochemical science & technology

247th ECS Meeting
Montréal, Canada
May 18-22, 2025
Palais des Congrès de Montréal

Showcase your science!

Abstract submission deadline extended: December 20

ECS UNITED

Laser-induced transformation of graphitic materials to two-dimensional graphene-like structures at ambient conditions

Aspasia Antonelou¹ , Vasiliki Benekou¹, Vassileios Dracopoulos¹,
Mary Kollia² and Spyros N Yannopoulos¹ 

¹ Foundation for Research and Technology Hellas—Institute of Chemical Engineering Sciences (FORTH/ICE-HT), PO Box 1414, GR-26504, Rio-Patras, Greece

² Laboratory of Electron Microscopy and Microanalysis, School of Natural Sciences, University of Patras, GR-26504, Rio-Patras, Greece

E-mail: sny@iceht.forth.gr

Received 28 March 2018, revised 15 June 2018

Accepted for publication 27 June 2018

Published 11 July 2018



CrossMark

Abstract

Laser processing of carbon compounds towards the formation of graphene-based structures gains ground in view of the practicality that lasers offer against other conventional graphene preparation methods. The current work explores the viability of low-cost lasers, operating at ambient conditions, for the transformation of various graphitic materials to structures with graphene-like atomic arrangements. Starting materials are at two opposing sides. On one side stands the typical graphite crystal with Bernal stacking and strong sp^2 character, while nanocrystalline graphitic powders are also investigated. It is demonstrated that graphene-like structures can be prepared either by starting from a well-organized Bernal-stacked network or by irradiating nanocrystalline carbon. The current findings document that laser processing at minimal chamber conditions shows high potential for preparing high-quality graphene-based structures starting from low-cost materials. Apart from being scalable, the proposed method is adaptable to current technological platforms emerging as a viable and eco-friendly graphene production technology.

Keywords: graphene, laser-growth, graphite

(Some figures may appear in colour only in the online journal)

1. Introduction

Graphene and graphene-based structures have emerged as key materials in numerous sectors of nanotechnology owing to their distinctive properties being potentially exploitable in a variety of applications in electronics, photonics, energy storage and conversion, membranes and coatings, sensors, etc [1–3]. Production technologies follow diverse approaches targeting on growing different forms of graphene suitable for particular applications. The current status shows that despite that graphene monolayer exhibits extraordinarily good electrical, optical, mechanical, etc properties, in the vast majority of possible viable applications with commercial success, other forms of graphene, i.e. graphene oxide, few and multilayer graphene-like structures, turbostratic graphene and so on, will

be utilized. This relieves most of the strict conditions for large area, defect-free monolayer graphene production, which has proven to be a formidable task. Laser processing has shown potential as a feasible technology for high-quality, cost-effective and environmentally friendly graphene production. Various laser sources have demonstrated capacity for high-quality graphene growth by properly processing inorganic, e.g. SiC decomposition [4–7], and organic compounds [8]. In addition, graphene growth by laser-assisted ablation of pyrolytic graphite targets has been explored; however, the graphene quality still remains very poor in addition to the fact that the final product contains also amorphous carbon and/or graphite crystals [9–12].

Transforming graphite—or other carbon forms—to graphene-like structures is yet a practically unexplored theme.

Graphite is the archetypal laminar structure. The weak inter-layer van der Waals forces are easily ruptured by external stimuli and the Bernal (ABAB...) stacking order disrupts giving rise to a transition from a three-dimensional (3D) structure to a two-dimensional (2D) arrangement. The co-existence of 3D and 2D phases in various forms of graphite has been known more than sixty years ago, when Franklin, using x-ray diffraction, showed that in such graphite specimens the intermediate value of the out-of-plane lattice parameters is an average value dictated by the relative fractions of the two phases. The structural basis of the 3D \rightarrow 2D graphite transition is the electronic decoupling of neighboring layers which ensues either when their distance increases or from rotational disorder, as already perceived by Franklin [13]. Similar effects were explored under a more rigorous basis for non-Bernal-stacked, multilayer graphene grown on the C-face of SiC [14, 15]. The appearance of Dirac-like electronic states in multilayer C-face rotationally faulted graphene, accounts for the origin of enhanced transport properties, which are comparable to those of the single-layer graphene [14, 15]. In summary, the 3D \rightarrow 2D transition in graphitic materials can, in principle, endow such structures with electronic properties similar to those of the single-layer and hence deserves further exploration.

The production of graphene-based structures from an inexpensive source such as graphite and other forms of carbon is a captivating, albeit challenging task. Here, we show that irradiation of graphite by a near-IR laser at practically ambient conditions can indeed result in the transformation of graphitic structures to graphene-like ones by electronically decoupling the graphite layers. Besides, proper irradiation of two commercially available carbon materials, namely, carbon black (Vulcan XC 72R from Cabot, used as support material in fuel cells) and activated carbon (Norit from Alfa Aesar) brings about a structural transformation from the nanocrystalline or amorphous-like state to an sp^2 bonding with inter-layer interactions different than those of Bernal-stacked graphite. In contrast to previous studies, emphasis is placed on the irradiated volume and not on the ablated material. For this reason, mechanisms describing the light-graphite interactions are discussed in some extent. Raman scattering and electron microscopies are used to explore the laser-induced morphological changes brought about to the irradiated volume so as to assess the quality of the graphene-like structures. We show that under irradiation at ambient conditions, graphite as well as other sp^3 carbon forms, can be transformed to good quality graphene-like structures using inexpensive laser equipment and a fast and environmentally friendly process.

2. Experimental

Various commercial carbon sources are used as starting materials. A graphite rod (Alfa Aesar 99.8% purity) is machined to disks which are used as targets for the irradiation procedure. Pieces of this material were also ground to powder and pressed to pellet for additional irradiation experiments.

The carbon nanopowders Norit (activated carbon, Alfa Aesar) and Vulcan (carbon black, XC 72R, Cabot) were pressed into small pellets to facilitate irradiation and electron microscopy. Large crystals of HOPG (Alfa Aesar) were exfoliated using scotch tape. Irradiation took place with the aid of Nd:YAG laser (Rofin, Desktop) operating at 1064 nm in the single shot rate, pulse width in the range 1–5 ms, and spot area diameter of 1 mm. Detailed fluence values are given in the relevant discussion. For all samples irradiation proceeded at ambient conditions; no vacuum or inert gases were used.

Electron microscopy images were collected with a high-resolution field-emission scanning electron microscope, (FE-SEM, (Zeiss, SUPRA 35VP) operated at 15 kV. Transmission electron microscope (TEM) and high-resolution TEM images were taken on a JEOL JEM-2100 transmission electron microscope operated at 200 kV. The sample for the TEM analysis was prepared by a standard procedure; the laser-processed powders were dispersed in ethanol by ultrasonic waves and spread onto a carbon-coated copper grid (200 mesh). Raman spectra were recorded with the 441.6 and the 514.5 nm laser lines as the excitation source. The scattered light was analyzed by the LabRam (Jobin-Yvon, HR800) and the T64000 (Jobin-Yvon) micro-Raman spectrometers at a spectral resolution of $\sim 2 \text{ cm}^{-1}$. A microscope objective with magnification 50 \times was used to focus the light onto a $\sim 2\text{--}3 \mu\text{m}$ spot. The light intensity was kept at low levels ($< 0.1 \text{ mW}$ on the sample) to avoid spectral changes due to heat-induced effects. The Raman shift was calibrated using the 520 cm^{-1} Raman band of crystalline Si.

3. Results and discussion

3.1. Graphite powder

Representative FE-SEM images of irradiated graphite are shown in figure 1. The insets in each image show a magnified view of the surface. Image 1(a) shows the typical crystal morphology of the pristine (unmodified) graphite target. Pristine graphite exhibits a compact structure with rather large crystalline grain sizes, where no exfoliated graphene layers are exposed. Irradiation dose increases in the series of the images 1(b)–(f). The FE-SEM images of the photo-processed graphite reveal that progressive morphological changes on the surface of the graphite grains take place, which are systematically evolving with the irradiation dose ranging from 100 to 260 J cm^{-2} . Appreciable exfoliation and modification of the compact graphite structure to more open textures are observed. Partially isolated graphene flakes protrude at the edges of the graphite grains for the highest irradiation dose used, see image 1(f).

More detailed quantitative information concerning the structural changes are provided by TEM and HR-TEM images as shown in figure 2. Image 2(a) is a high magnification micrograph of a photo-processed graphite grain using 260 J cm^{-2} . The high transparency of the material indicates the formation of a very distorted graphitic structure with appreciable exfoliation of the graphene layers. Images 2(b)–(d)

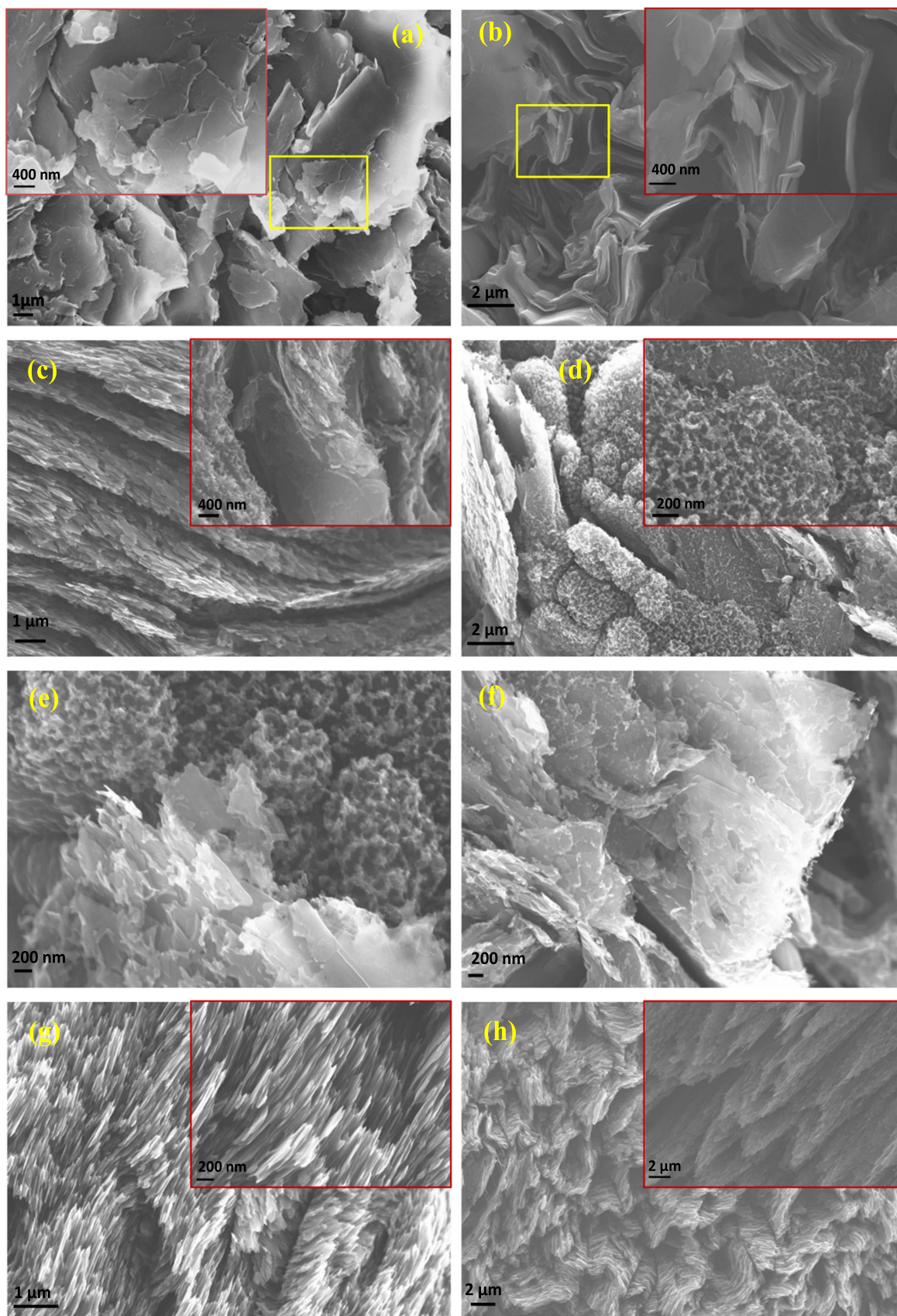


Figure 1. FE-SEM images of irradiated graphite crystals. (a) Pristine material. The morphology change of the photo-processed material is shown with increasing laser fluence from (b) to (f) in the following way (b) 100, (c) 150, (d) 150, (e) 200, (f) 200 (g) 260, and (h) 260 J cm^{-2} .

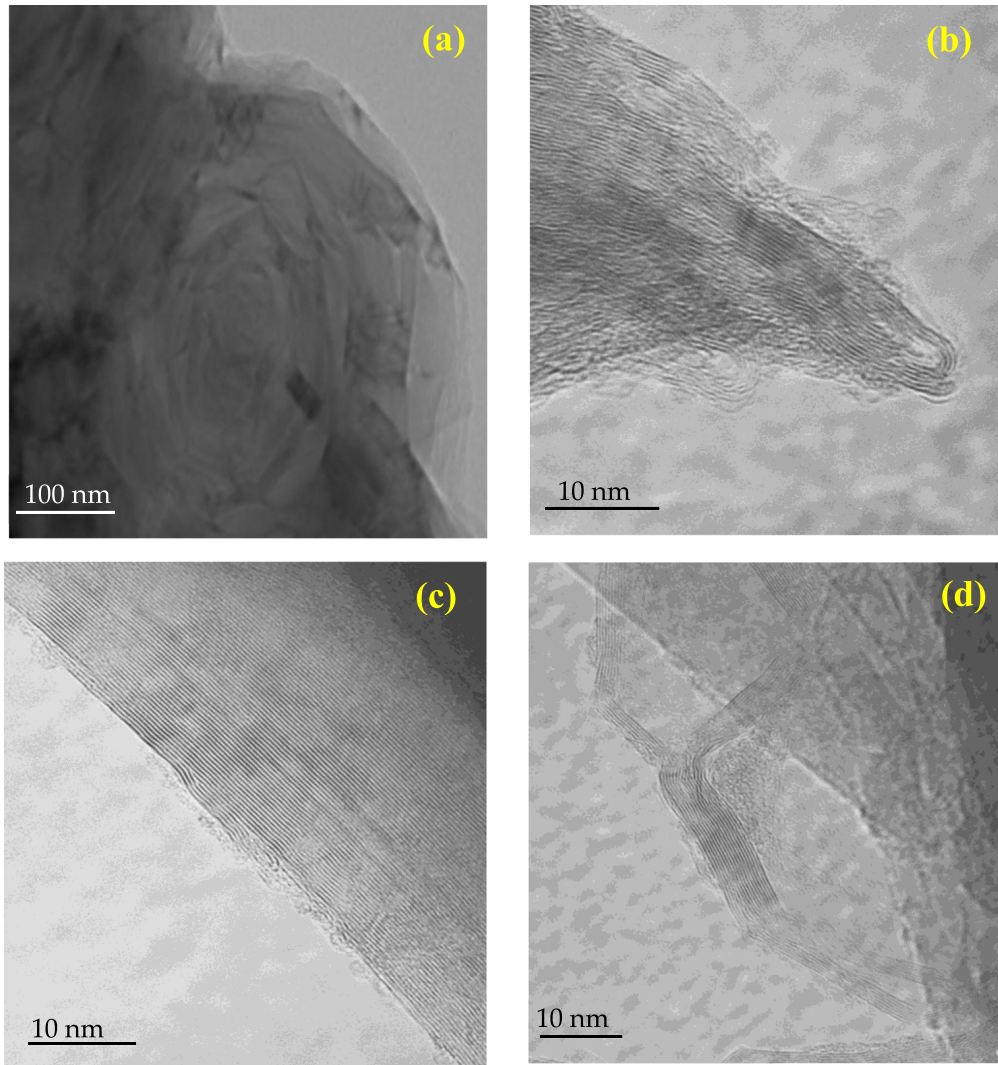


Figure 2. TEM images of irradiated graphite crystals using 260 J cm^{-2} . (a) Low magnification image. (b)–(d) Selected high-resolution images showing the graphene layers.

show the high-resolution structure of various irradiated structures. High extent of layer exfoliation and substantial widening of the interlayer distance is observed. Quantitative information is provided in figure 3, where the interlayer distance is shown, provided directly from the high-resolution images and from electron diffraction patterns. Figure 3(a) displays the $d(002)$ interlayer spacing as estimated by the HR-TEM images; the data points for various measurements corresponds to an average spacing of several consecutive layers to minimize the error. In all cases the estimated interlayer distances are far larger than the nominal value of graphite, i.e. 0.335 nm, shown by the horizontal dashed line. The average value is $\langle d(002) \rangle = 0.380 \pm 0.031 \text{ nm}$, demonstrating severe interlayer expansion of the irradiated graphite crystals. For comparison, the interlayer distances of the pristine (not irradiated) sample are also shown in this figure revealing the proximity of these values to the nominal one. Figure 3(b) shows the interlayer distance as estimated by the electron diffraction patterns. Again, the $d(002)$ values of the laser-processed sample are systematically higher

than the corresponding values of pristine graphite; the latter fits well the nominal value of 0.335 nm.

To get a deeper understanding about the changes in the atomic structures, basically to retrieve information on the layer stacking order, Raman spectroscopy is used as it stands as one of the most versatile technique for fast monitoring atomic arrangement in carbon. A large number of Raman spectra were recorded for each sample; representative spectra of the pristine graphite and the laser-processed material are shown in figure 4. Light fluence values are denoted in the figure caption. From bottom to top the spectra are arranged in an order of increasing the symmetrical Lorentzian character of the 2D band. The spectrum in the bottom (a) corresponds to the Raman spectrum of highly-ordered pyrolytic graphite where the 2D band displays the typical low energy shoulder, which accounts for almost one third to one second of the high energy peak intensity. Two types of changes in the Raman spectra are observed. The first concerns the emergence of new weak Raman bands situated in the high energy region

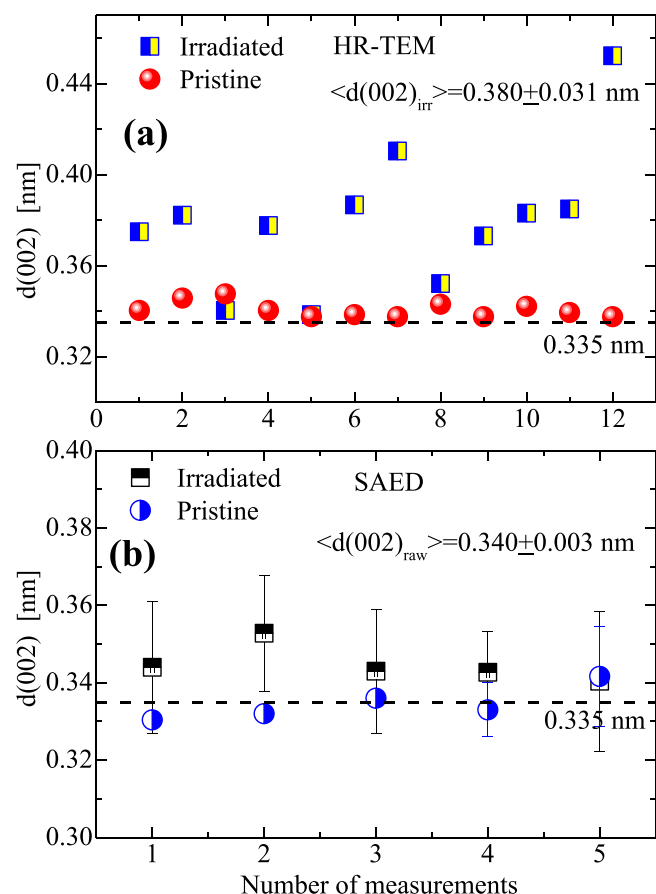


Figure 3. Interlayer spacing of irradiated (using 260 J cm^{-2}) and pristine graphite as estimated by the HR-TEM images (a), and the electron diffraction patterns (b). The horizontal dotted lines represent the interlayer spacing of pristine graphite.

($>2900 \text{ cm}^{-1}$) and the second relates to the shape of 2D band located in the spectral window $2600\text{--}2900 \text{ cm}^{-1}$. As the spectral profile of the 2D band becomes progressively more Lorentzian, two new weak bands at $\sim 2965 \text{ (D + G)}$ and 3172 cm^{-1} appear in the Raman spectrum. The $2\text{D}'$ sharp band of HOPG at 3242 cm^{-1} becomes gradually broader from bottom to top in figure 4. The spectrum shown as dots in panel (f), recorded with the 514.5 nm wavelength, is characterized by a strong and very narrow 2D band. Such spectra were measured sporadically in the irradiated area denoting the formation of very high-quality graphene structures. More quantitative information about the change of the spectral profile of the 2D band is shown in figure 5 where the spectra have been fitted by Lorentzian lines. The spectrum of HOPG is fitted by two Lorentzian lines separated by $\sim 40 \text{ cm}^{-1}$. For the irradiated material, a new band appears situated in the middle of the two bands of HOPG.

It would be instructive at this point to briefly survey on the local atomic structure of various types of graphite by Raman scattering. Several such studies have contributed to our knowledge of the structure of different graphitic forms [16–24]. Lespade *et al* [18] was among the first who explored in detail the spectral features of the G and 2D bands and their dependence in relation to the interlayer spacing. They reported the spectral change of the 2D Raman band from a doublet to a

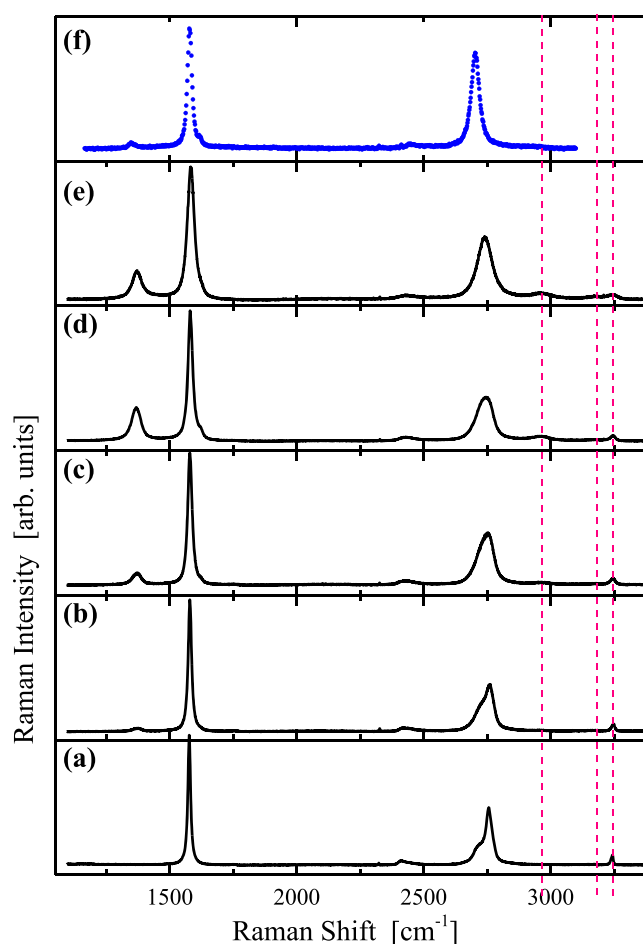


Figure 4. Raman spectra of (a) pristine HOPG and various irradiated graphite materials from (b) to (f). Spectra (e) and (f) exhibit single Lorentzian character of the 2D band. Irradiation conditions are as follows: (b) 100, (c) 150, (d) 200, (e) 260, (f) 260 J cm^{-2} .

single Lorentzian line when the interlayer spacing distance exceeds c.a. 3.38 \AA . Studying five different graphite types with varying 2D to 3D volume fractions, Wilhelm *et al* [19] noticed three features in the Raman spectra for graphitic materials with dominant 2D structures: (i) a stronger (than all other structures) Raman intensity of the G-band, (ii) a single Lorentzian shape of the 2D band, and (iii) the presence of a weak band located at $\sim 3185 \text{ cm}^{-1}$. Barros *et al* [20] identified three lines under the 2D band lineshape; one is assigned to contributions from 2D structures, $2\text{D}^{(2\text{D})}$, and two lines are assigned to 3D arrangements $2\text{D}_1^{(3\text{D})}$ and $2\text{D}_2^{(3\text{D})}$ separated by $\sim 55\text{--}60 \text{ cm}^{-1}$ while the $2\text{D}^{(2\text{D})}$ is situated in between the two lines of the 3D structure. Along the same line, Cancado *et al* [23] showed more quantitatively that Raman scattering can be used to monitor with good accuracy the degree of stacking order in graphitic materials. Finally, a more detailed description of polycrystalline graphene structures was recently provided by Ribeiro-Soares *et al* [24] based on a model that considers also the width of the crystallite grain boundary. Useful relations between structural correlation lengths and spectral parameters of Raman bands were proposed.

Figure 5 presents analysis of the 2D band spectral range of the Raman spectra shown in figure 4 based on the band

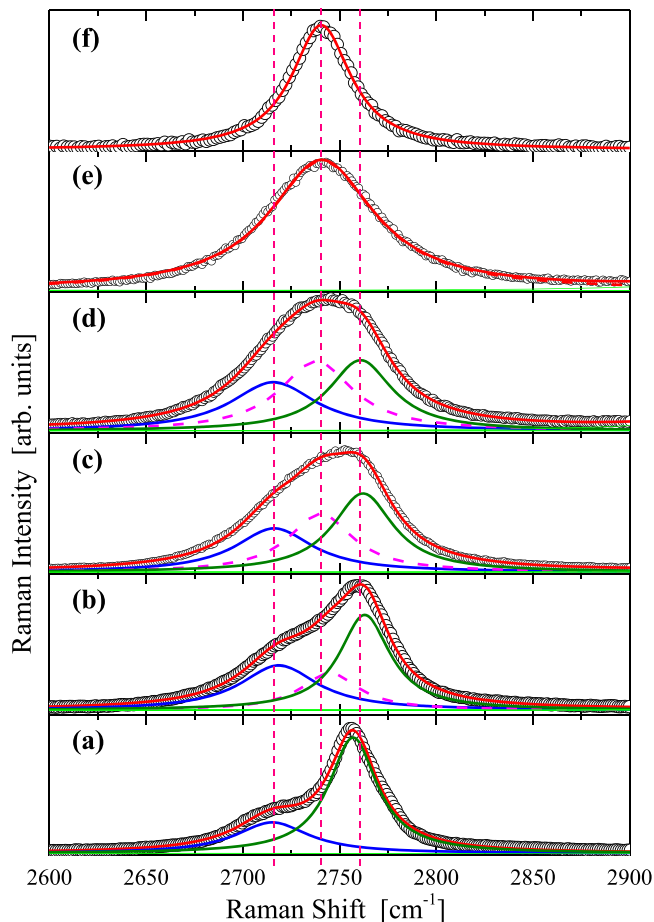


Figure 5. Analysis of the 2D band of the Raman spectra shown in figure 4, into its various components as described in the text. Open circles: experimental data; thick solid line: best fit curve. Irradiation conditions are as follows: (b) 100, (c) 150, (d) 200, (e) 260, (f) 260 J cm^{-2} .

assignment mentioned above. The spectrum at the bottom represents HOPG and the deconvolution (using Origin Lab 7.5) results typically in two Lorentzian lines. Retaining the notation of Cancado *et al* [23] we symbolize the HOPG bands in figure 5 as $2D_A^{(3D)}$ and $2D_B^{(3D)}$, and the band emerging at $\sim 2740 \text{ cm}^{-1}$ as $2D^{(2D)}$. From bottom to top we observe a progressive increase of the new band at $\sim 2740 \text{ cm}^{-1}$. The gradual transformation of 3D to 2D graphite is manifested by the dominance of the $2D^{(2D)}$ band where the 2D band envelope reverts to a single Lorentzian form, as is the case of turbostratic graphene characterized by a FWHM of $\sim 65 \text{ cm}^{-1}$, figure 5(e). For certain cases (top spectrum) the 2D band becomes very narrow, i.e. with a FWHM of 37 cm^{-1} , approaching that of monolayer graphene. The very large interlayer distance of certain regions of irradiated graphite (figure 3) is evidently the cause of this observation. This transition to a single Lorentzian signifies the exfoliation of graphene layers to such extent that no electronic coupling to neighboring layers any longer exists [14]. As Franklin [13] has reported, the transition to ‘non-graphitic’ carbon or ‘orientation’ to ‘disorientation’ transition, occurs for interlayer spacing exceeding the threshold of 0.344 nm. Partially

graphitic carbons have spacing between the graphite value 0.335 nm and the above threshold value 0.344 nm.

The structural transformation described above is further manifested in the broadening of the G-band, which becomes systematically broader when the fraction of the 3D structure increases. This finding is in harmony with a correlation between the FWHM of the G-band with the interlayer spacing $d(002)$ as reported by Yoshida *et al* [25]. Indeed, the data of the current work show that the FWHM of the G-band increases almost linearly from 13 to 33 cm^{-1} for the spectra that correspond from (a) to (f), respectively in figure 5. Based on the aforementioned correlation between the width of the G-band and $d(002)$, a broadening of 33 cm^{-1} implies an interlayer spacing of ca 0.342 nm. This result is in accord with the increased spacing estimated by HR-TEM.

3.2. Highly-ordered pyrolytic graphite

Attempts to modify the structure of HOPG by changing the interlayer spacing were not as successful as in the case of graphite powder. The much higher ablation rate of HOPG, compared to graphite powder, prevents from producing a suitably modified material by irradiation. HOPG is easily ablated even with the mildest conditions, 35 J cm^{-2} , which does not permit the study of the irradiated area. Indeed, based on ablation mechanisms proposed by atomistic simulations [26] the ordered layer structure can rather readily be subjected to large oscillations at a direction normal to the plane originating from a non-equilibrium charge distribution developed upon irradiation. For the current work, a HOPG sample, several layers thick, was prepared by mechanical exfoliation from a large crystal using the typical procedure of scotch tape. The main reason was to obtain a fresh, flat surface in order to facilitate the observation of post-irradiated morphological changes. The sample was covered with a glass slide and was subjected to irradiation. Even at low fluences where the graphite powder exhibits practically no ablation, the HOPG flakes are completely removed from the irradiated area and the ablated product condensates on the glass slide.

Figure 6 shows typical Raman spectra of the ablated material on the glass cover, i.e. (a) and (b), and spectra taken from the periphery of the irradiated area showing the structural change of the photo-processed but not ablated HOPG (c). Judging from the moderate intensity of the D band and the symmetric spectral shape of the 2D band, spectra (a) and (b) in figure 6 demonstrate that high-quality graphene-like structures emerge as the ablation product of HOPG, even at ambient conditions. Based on the Raman spectra and the criteria mentioned in previous sections concerning the relation between spectra features and the quality of graphene-like structures, it becomes evident that the deposited graphitic material in the current work is of much higher quality than the ablated films deposited by ns and ps lasers [9–12] under ultrahigh vacuum conditions. However, the optimization of the process for improving the quality of the ablated material goes beyond the scope of the current work. The symmetric 2D band of the Raman spectrum of irradiated HOPG shown

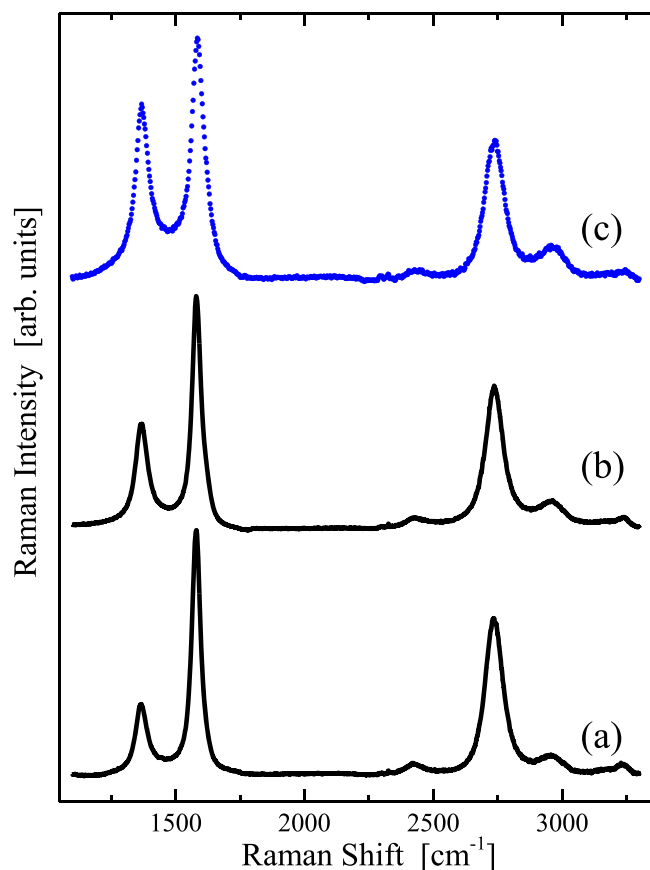


Figure 6. Raman spectra of irradiated HOPG (35 J cm^{-2}): (a) and (b) correspond to spectra collected from the ablated product; (c) denotes a spectrum collected at the periphery of the irradiated spot.

in figure 6(c) shows modification of the Bernal stacking. Apparently, this is accompanied with a higher defect density in comparison to pristine HOPG. Figure 7 shows FE-SEM images of the HOPG surface prior to excitation (a) and the ablated product, 35 J cm^{-2} , collected on the glass substrate (b). This comparison reveals the dense well-packed structure of untreated HOPG, where some surface layers exhibit wrinkled morphology, while the ablated material (b) shows a rather porous structure, vastly different than that of the HOPG. In summary, irradiation under the conditions of the present study shows that HOPG exhibits much faster ablation rate than powder graphite while the remaining photo-processed material adopts a different structure as regards the interlayer spacing.

3.3. Commercially available carbon nanopowders

Irradiation of carbon black (Vulcan) and activated carbon (Norit) powders yielded interesting results as these two predominantly nanocrystalline graphite forms transform readily to sp^2 networks. The XRD data of Vulcan and Norit presented in figures 8(a) and 9(a), respectively, demonstrate that these materials bear a structure between that of a graphitic material and amorphous carbon. Few sharp Bragg peaks in the XRD pattern of Norit (denoted by asterisks) originate from impurities. The particles of Vulcan powder are spherical with

primary particle size in the range of 30–60 nm and the specific surface area is relatively large ($218 \text{ m}^2 \text{ g}^{-1}$).

Raman spectra of both pristine powders shown in figures 8(b) and 9(b), respectively, illustrate in accordance with the XRD data an amorphous-like or nanocrystalline structure of the materials, as is evident from the enhanced sp^3 bonding. Representative Raman spectra for both powders after irradiation show a drastic structural transformation of the amorphous-like or nanocrystalline structure to a more ordered atomic arrangement with predominantly sp^2 character. Vulcan requires appreciably higher fluence than Norit, 400 and 50 J cm^{-2} , respectively, to be transformed in the form that Raman spectra show. The most striking effect is the development of an intense, symmetric 2D band. The appreciable weakening of the D band intensity and the narrowing of both the D and G bands, manifest the improvement of crystal quality and increase of the crystal size. It is also observed that the G-band for both Vulcan and Norit exhibits redshift for more than 10 cm^{-1} upon irradiation. This is in accord with the diminishing of the nanocrystalline or sp^3 character of the material according to the model by Ferrari and Robertson [27]. In a recent study, tetrahedrally amorphous carbon was irradiated by nano- and femtosecond laser pulses, hence being transformed to a more graphitic structure [28]. However, judging from the Raman spectra, even in the best case the degree of sp^2 formation in that work is inferior to the transformation achieved in the current study. In addition, no evolution of the 2D band was reported. The morphological changes brought about by irradiation in these powders are shown in figures 7(c) and (d) for pristine and irradiated Vulcan and (e) and (f) for pristine and irradiated Norit, respectively.

4. Atomic-scale mechanism of the laser-assisted graphene layer exfoliation

The effect of laser irradiation on the structure of graphite is a long standing theme explored both experimentally and theoretically. In the vast majority of studies, the main focus was on the controlled ablation of graphite towards formation of few layer graphene structures on various substrates held at certain distance away from the target. No report, to our knowledge, has been published up until now pertaining to transformation of the atomic arrangement of the irradiated target into graphene-like configurations.

Both temperature and pressure effects have been invoked to account for the observed structural changes of irradiated graphite targets. Speck *et al* [29] found that apart from certain morphological changes, i.e. formation of carbon spheroids, the resolidification of the material that melts under irradiation turns to turbostratic order with layers being randomly rotated and translated. Simulation approaches have shown that there exists an energy threshold which signifies the change of the ablation mechanism [30]. For low fluence, the photoinduced electron-hole plasma leads to vibrational excitation of the graphene layers, hence increasing the separation between them and reducing their

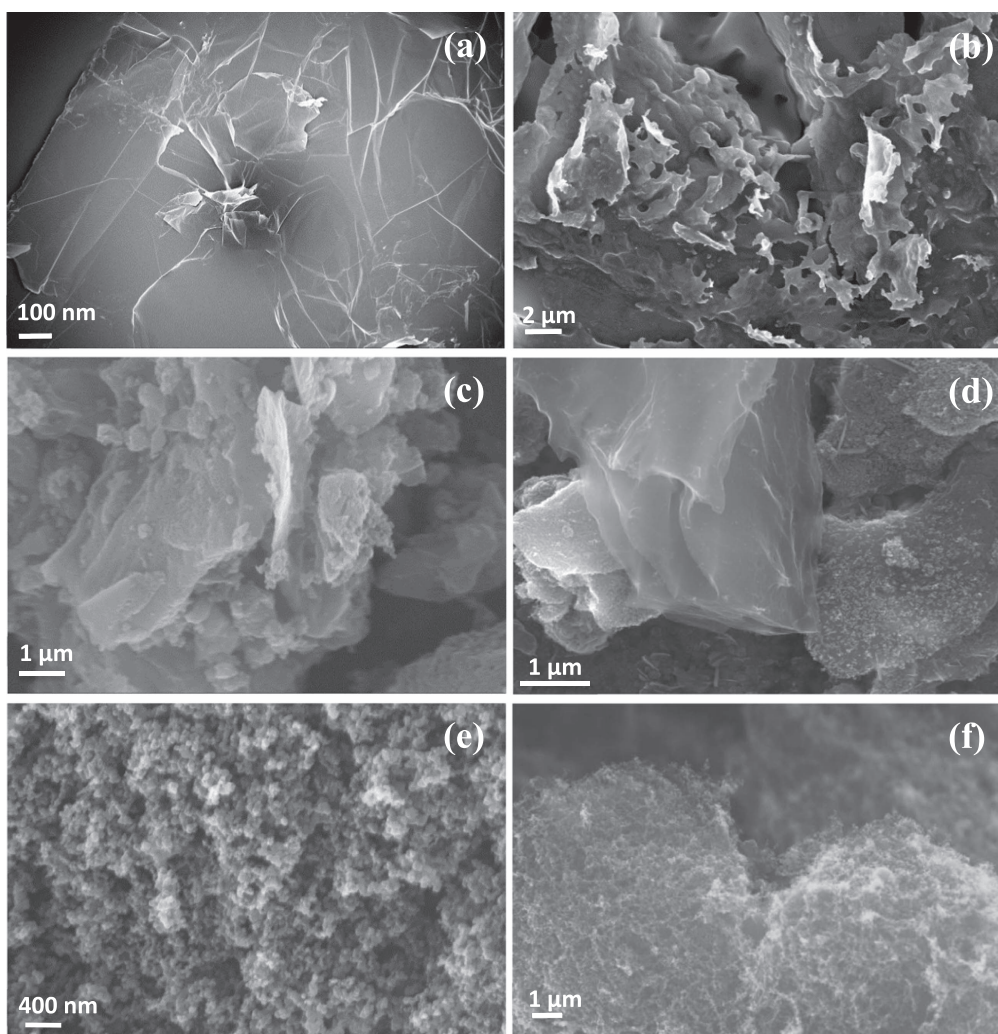


Figure 7. FE-SEM images of pristine (left column) and irradiated (right column) materials. (a) and (b) HOPG, 35 J cm^{-2} ; (c) and (d) Vulcan, 400 J cm^{-2} ; (e) and (f) Norit, 50 J cm^{-2} .

interaction. In this context, intact layers can exfoliate from the surface of the material. For high fluence, non-equilibrium melting leads to fast evaporation and disintegration of the material.

Direct observation of the transient changes in the graphite structure followed by photoexcitation revealed that light repopulates the electronic states and causes charge redistribution on the surface [31]. In this way, a Coulomb field is created on the irradiated surface layers. Transient states with sp^3 type interlayer bonding were also observed. Ultrafast ablation of graphite studied by time-of-flight spectroscopy showed that charged carbon products escape from the surface upon irradiation [32]. Coulomb explosion was considered to account for the observed effect. Fragmentary intact-sheet ablation of double-layer graphite by fs-laser excitation has been observed experimentally and studied by simulations. The double-layer ablation effect is considered to be facilitated by the formation of interlayer bonding [33]. Those findings provided some indication that the ablation does not simply arise from the strong repulsion between different planes,

resulting from a decrease of their distance as suggested elsewhere [30, 34].

The above-mentioned brief discussion on a number of experimental and simulation studies reveals that a wealth of mechanisms has over several years proposed to account for existing experimental data or to put forward ideas that await verification or disproof from experiments. The current work provides solid evidence that under minimal conditions of the irradiation experiment (i.e. ambient atmosphere, cost-effective, fast and scalable) graphene-like structures can be prepared either by starting from a well-organized Bernal-stacked network or by irradiating amorphous forms of carbon. In the former, moderate structural changes take place substantiated by an expansion of the interlayer spacing while bearing negligible effects on the sp^2 network. Coulomb expansion could possibly rationalize the observed effects. Expansion of the interlayer spacing of graphite confers on it electronic decoupling between layers; hence, conductivity enhancement is expected according to theoretical predictions [14, 15]. As

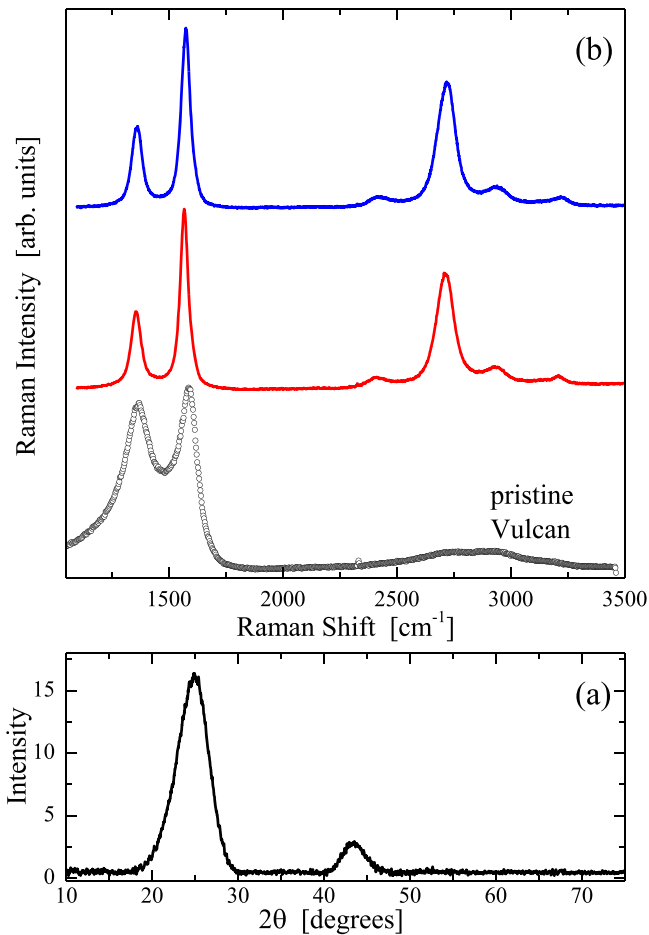


Figure 8. (a) XRD pattern of Vulcan. (b) Raman spectra of pristine and irradiated Vulcan (400 J cm^{-2}).

regards amorphous carbon forms, reorganization of the atomic arrangement takes place, mediated via a substantial sp^3 to sp^2 transformation which entails crystallization of the initial quasi-amorphous material. In this case, the underlying mechanism responsible for the growth of large crystal domains is less clear. Several studies have been conducted using ns, ps, and fs lasers [28, 35, 36]. Nonlinear effects and plasma-mediated ablation processes have been invoked to account for the fs-laser processing. For all laser pulse durations, from ns to fs, an sp^3 to sp^2 transformation is observed. The current results and the aforementioned discussion makes it obvious that no common mechanism can be contemplated to account for the transformation of the various graphite forms to graphene-like structures. The starting materials have vastly contrasting atomic arrangement structure, morphology and physical properties, while irradiation reconfigures the atomic arrangement towards very similar structures, irrespective of the starting material. Apart from that the proposed process takes place at ambient conditions, a key advantage of our experimental approach is that the laser-assisted changes to graphene-like structures pertain to the irradiated area, and not to the ablated product at a substrate placed away from the target. This endows the process adaptability to current

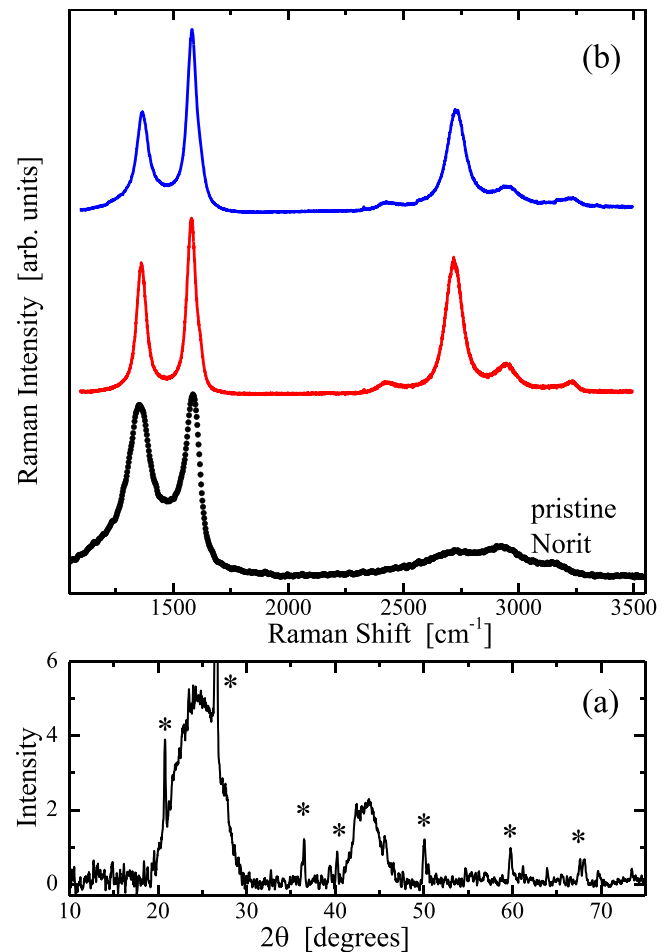


Figure 9. (a) XRD pattern of Norit. (b) Raman spectra of pristine and irradiated Norit (50 J cm^{-2}).

technologies where *in situ* writing graphene-based structures on a device is required.

5. Conclusions

In summary, we have shown that—using low-cost laser sources under minimal irradiation conditions, i.e. with no strict chamber condition such as vacuum or inert gases—various forms of elemental carbon can be transformed to graphene-like structures. Unlike the vast majority of the previous studies which concentrate on the ablated product deposited on a substrate, the current work places the emphasis on the irradiated target. The main purpose of the current work was to demonstrate that under the simple conditions used, graphene-like structures with well resolved 2D band in their Raman spectra can be obtained either starting from a well-organized sp^2 network or from a disordered graphitic form such as carbon black and activated carbon. Coulomb expansion was envisaged as a possible mechanism for the interlayer expansion of the well-organized sp^2 network as observed by TEM in irradiated graphite and indirectly inferred from the increase of the $2D^{(2D)}$ component at the expense of the



$2D_1^{(3D)}$ and $2D_2^{(3D)}$ components. This signifies a structural transformation from 3D to 2D arrangement. This structural change is expected to modify electronic properties, as simulations and experiments have shown that loss of Bernal stacking electronically decouples neighboring layers. Therefore, the repulsive Coulomb interaction developed after photoexcitation competes the attractive weak van der Waal forces ending up to increased interlayer spacing. For the nanocrystalline or quasi-amorphous carbons forms an extensive sp^3 to sp^2 transformation is observed leading to a sp^2 structure with non-Bernal stacking and an intense 2D band in the Raman spectrum.

As a final remark we would like to state that laser-assisted growth of graphene-based materials can be transformed to a viable technology for large-scale reliable production. On its own right, the method is versatile since it can be adapted to existing platforms for directly 'writing' graphene into a device, thus surpassing other chemical and high-temperature based methods. In addition, unlike previous reports which use expensive equipment (i.e. fs-laser sources) operating with beams focused at the micron scale, rendering the whole process slow and costly, the current experimental scheme employs a laser source widely used in the marking/welding industry. The writing spot size can be adjusted to be in the few mm scale, thus being orders of magnitudes faster than other laser-assisted methods reported up until now. In this context, the process is intrinsically scalable and eco-friendly as no pre- or post-treatment with solvents and other chemicals is required.

Acknowledgments

We acknowledge support of this work from the project 'AENAO—Materials and processes for energy and environmental applications' (MIS 5002556) which is implemented under the 'Action for the Strategic Development on the Research and Technological Sector', funded by the Operational Programme 'Competitiveness, Entrepreneurship and Innovation' (NSRF 2014-2020) and co-financed by Greece and the European Union (European Regional Development Fund).

ORCID iDs

Aspasia Antonelou  <https://orcid.org/0000-0002-3276-9127>
 Spyros N Yannopoulos  <https://orcid.org/0000-0001-6684-3172>

References

- [1] 2014 Focus issue: graphene applications *Nat. Nanotechnol.* **9** 726–807 (<https://nature.com/nnano/focus/graphene-applications/index.html>)
- [2] Novoselov K S, Fal'ko V I, Colombo L, Gellert P R, Schwab M G and Kim K 2012 A roadmap for graphene *Nature* **490** 192–200
- [3] Avouris P and Dimitrakopoulos C 2012 Graphene: synthesis and applications *Mater. Today* **15** 86–97
- [4] Yannopoulos S N, Siokou A, Nasikas N K, Dracopoulos V, Ravani F and Papatheodorou G N 2012 CO₂-laser-induced growth of epitaxial graphene on 6H–SiC(0001) *Adv. Funct. Mater.* **22** 113–20
- [5] Antonelou A, Dracopoulos V and Yannopoulos S N 2015 Laser processing of SiC: from graphene-coated SiC particles to 3D graphene froths *Carbon* **85** 176–84
- [6] Lee S *et al* 2010 Laser-synthesized epitaxial graphene *ACS Nano*. **4** 7524–30
- [7] de A M Galvão N K, de Vasconcelos G, dos Santos M V R, Campos T M B, Pessoa R S, Guerino M, Djouadi M A and Maciel H S 2016 Growth and characterization of graphene on polycrystalline SiC substrate using heating by CO₂ laser beam *Mater. Res.* **19** 1329–34
- [8] Chyan Y, Ye R, Li Y, Singh S P, Arnusch C J and Tour J M 2018 Laser-induced graphene by multiple lasing: toward electronics on cloth, paper, and food *ACS Nano* **12** 2176–83
- [9] Cappelli E, Scilletta C, Servidori M, Valentini V and Orlando S 2008 Morphology, structure and density evolution of carbon nano-structures deposited by N-IR pulsed laser ablation of graphite *Diam. Relat. Mater.* **17** 1476–81
- [10] Wang K, Tai G, Wong K H, Lau S P and Guo W 2011 Ni induced few-layer graphene growth at low temperature by pulsed laser deposition *AIP Adv.* **1** 022141
- [11] Qian M, Zhou Y S, Gao Y, Park J B, Feng T, Huang S M, Sun Z, Jiang L and Lu Y F 2011 Formation of graphene sheets through laser exfoliation of highly ordered pyrolytic graphite *Appl. Phys. Lett.* **98** 173108
- [12] Koh A T T, Foong Y M and Chua D H C 2010 Cooling rate and energy dependence of pulsed laser fabricated graphene on nickel at reduced temperature *Appl. Phys. Lett.* **97** 114102
- [13] Franklin R E 1951 The structure of graphitic carbons *Acta Crystallogr.* **4** 253–61
- [14] Hass J, Varchon F, Millán-Otoya J E, Sprinkle M, Sharma N, de Heer W A, Berger C, First P N, Magaud L and Conrad E H 2008 Why multilayer graphene on 4 H–SiC (000 $\bar{1}$) behaves like a single sheet of graphene *Phys. Rev. Lett.* **100** 125504
- [15] Pankratov O, Hensel S and Bockstedte M 2010 Electron spectrum of epitaxial graphene monolayers *Phys. Rev. B* **82** 121416
- [16] Tuinstra F and Koenig J L 1970 Raman spectrum of graphite *J. Chem. Phys.* **53** 1126–30
- [17] Nemanich R J and Solin S A 1979 First- and second-order Raman scattering from finite-size crystals of graphite *Phys. Rev. B* **20** 392–401
- [18] Lespade P, Marchand A, Couzi M and Cruege F 1984 Caractérisation de matériaux carbonés par microspectrométrie Raman *Carbon* **22** 375–85
- [19] Wilhelm H, Lelaurain M, McRae E and Humbert B 1998 Raman spectroscopic studies on well-defined carbonaceous materials of strong two-dimensional character *J. Appl. Phys.* **84** 6552–8
- [20] Barros E B, Demir N S, Souza Filho A G, Mendes Filho J, Jorio A, Dresselhaus G and Dresselhaus M S 2005 Raman spectroscopy of graphitic foams *Phys. Rev. B* **71** 165422
- [21] Ferrari A C *et al* 2006 Raman spectrum of graphene and graphene layers *Phys. Rev. Lett.* **97** 187401
- [22] Cançado L G, Takai K, Enoki T, Endo M, Kim Y A, Mizusaki H, Jorio A, Coelho L N, Magalhães-Paniago R and Pimenta M A 2006 General equation for the determination of the crystallite size L_a of nanographite by Raman spectroscopy *Appl. Phys. Lett.* **88** 163106
- [23] Cançado L G, Takai K, Enoki T, Endo M, Kim Y A, Mizusaki H, Speziali N L, Jorio A and Pimenta M A 2008 Measuring the degree of stacking order in graphite by Raman spectroscopy *Carbon* **46** 272–5

- [24] Ribeiro-Soares J et al 2015 Structural analysis of polycrystalline graphene systems by Raman spectroscopy *Carbon* **95** 646–52
- [25] Yoshida A, Kaburagi Y and Hishiyama Y 2006 Full width at half maximum intensity of the G band in the first order Raman spectrum of carbon material as a parameter for graphitization *Carbon* **44** 2333–5
- [26] Bennemann K H 2011 Photoinduced phase transitions *J. Phys.: Condens. Matter* **23** 073202
- [27] Ferrari A C and Robertson J 2000 Interpretation of Raman spectra of disordered and amorphous carbon *Phys. Rev. B* **61** 14095–107
- [28] Arutyunyan N R, Komlenok M S, Zavedeev E V and Pimenov S M 2018 Raman spectroscopy of amorphous carbon films modified by single-pulse irradiation of nanosecond and femtosecond lasers *Phys. Status Solidi* **255** 1700225
- [29] Speck J S, Steinbeck J and Dresselhaus M S 1990 Microstructural studies of laser irradiated graphite surfaces *J. Mater. Res.* **5** 980–8
- [30] Jeschke H O, Garcia M E and Bennemann K H 2001 Theory for the ultrafast ablation of graphite films *Phys. Rev. Lett.* **87** 015003
- [31] Raman R K, Murooka Y, Ruan C-Y, Yang T, Berber S and Tománek D 2008 Direct observation of optically induced transient structures in graphite using ultrafast electron crystallography *Phys. Rev. Lett.* **101** 077401
- [32] Lenner M, Kaplan A, Huchon C and Palmer R E 2009 Ultrafast laser ablation of graphite *Phys. Rev. B* **79** 184105
- [33] Ohnishi H, Inami E and Kanasaki J 2011 Intact-sheet double-layer ablation induced by femtosecond-laser excitation of graphite *Surf. Sci.* **605** 1497–502
- [34] Miyamoto Y, Zhang H and Tománek D 2010 Photoexfoliation of graphene from graphite: an *ab initio* study *Phys. Rev. Lett.* **104** 208302
- [35] Kononenko T V, Kononenko V V, Pimenov S M, Zavedeev E V, Konov V I, Romano V and Dumitru G 2005 Effects of pulse duration in laser processing of diamond-like carbon films *Diam. Relat. Mater.* **14** 1368–76
- [36] Roch T, Lasagni A and Beyer E 2011 Nanosecond UV laser graphitization and delamination of thin tetrahedral amorphous carbon films with different sp³/sp² content *Thin Solid Films* **519** 3756–61